Resource

Cell Reports

A Single-Cell Model for Synaptic Transmission and Plasticity in Human iPSC-Derived Neurons

Graphical Abstract

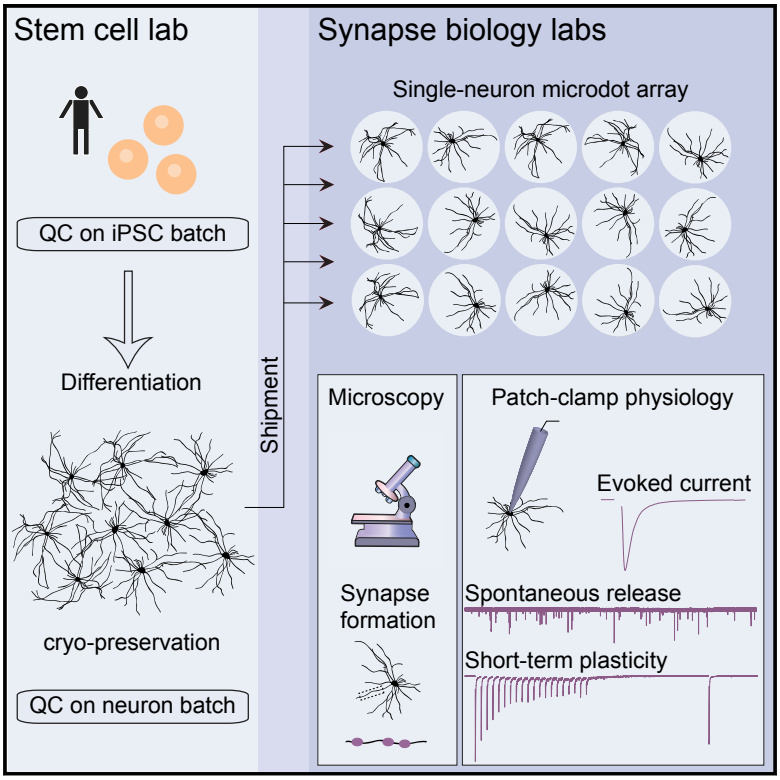

Highlights

- We establish a single-cell model to study synapses in iPSC-derived neurons
- This platform allows quantitative analysis of synaptic transmission and plasticity
- The platform is validated for GABA- or glutamatergic iPSC-derived human neurons
- The platform is scalable and suitable for compound screening and disease modeling

Authors

Marieke Meijer, Kristina Rehbach, Jessie W. Brunner, ..., Ruud F. Toonen, Oliver Brüstle, Matthijs Verhage

Correspondence

peitz@uni-bonn.de (M.P.), brustle@uni-bonn.de (O.B.), matthijs@cncr.vu.nl (M.V.)

In Brief

This multisite study by Meijer et al. establishes a standardized *in vitro* approach to study synapse formation and function in single iPSC-derived human neurons. They validate this approach for GABA and glutamatergic human neurons. The methodology is scalable and suitable for compound screening and disease modeling.

Meijer et al., 2019, Cell Reports *27*, 2199–2211
May 14, 2019
https://doi.org/10.1016/j.celrep.2019.04.058

CellPress

Cell Reports
Resource

A Single-Cell Model for Synaptic Transmission and Plasticity in Human iPSC-Derived Neurons

Marieke Meijer,[1,8] Kristina Rehbach,[3,5,8] Jessie W. Brunner,[2] Jessica A. Classen,[2] Hanna C.A. Lammertse,[1] Lola A. van Linge,[2] Desiree Schut,[1] Tamara Krutenko,[3] Matthias Hebisch,[3] L. Niels Cornelisse,[1] Patrick F. Sullivan,[6,7] Michael Peitz,[3,4,*] Ruud F. Toonen,[2] Oliver Brüstle,[3,*] and Matthijs Verhage[1,2,9,*]

[1]Department of Clinical Genetics, Center for Neurogenomics and Cognitive Research (CNCR), VU University Amsterdam and VU Medical Center, de Boelelaan 1085, 1081 HV Amsterdam, the Netherlands
[2]Department of Functional Genomics, Center for Neurogenomics and Cognitive Research (CNCR), VU University Amsterdam and VU Medical Center, de Boelelaan 1085, 1081 HV Amsterdam, the Netherlands
[3]Institute of Reconstructive Neurobiology, University of Bonn School of Medicine & University Hospital Bonn, Bonn, Germany
[4]Cell Programming Core Facility, University of Bonn School of Medicine, Bonn, Germany
[5]LIFE&BRAIN GmbH, Cellomics Unit, 53127 Bonn, Germany
[6]UNC Center for Psychiatric Genomics, University of North Carolina at Chapel Hill, 101 Manning Drive, Chapel Hill, NC 27599-7160, USA
[7]Karolinska Institutet, Department of Medical Epidemiology and Biostatistics and Department of (Clinical) Genetics, Nobels Väg 12A, 171 77 Stockholm, Sweden
[8]These authors contributed equally
[9]Lead Contact
*Correspondence: peitz@uni-bonn.de (M.P.), brustle@uni-bonn.de (O.B.), matthijs@cncr.vu.nl (M.V.)
https://doi.org/10.1016/j.celrep.2019.04.058

SUMMARY

Synaptic dysfunction is associated with many brain disorders, but robust human cell models to study synaptic transmission and plasticity are lacking. Instead, current *in vitro* studies on human neurons typically rely on spontaneous synaptic events as a proxy for synapse function. Here, we describe a standardized *in vitro* approach using human neurons cultured individually on glia microdot arrays that allow single-cell analysis of synapse formation and function. We show that single glutamatergic or GABAergic forebrain neurons differentiated from human induced pluripotent stem cells form mature synapses that exhibit robust evoked synaptic transmission. These neurons show plasticity features such as synaptic facilitation, depression, and recovery. Finally, we show that spontaneous events are a poor predictor of synaptic maturity and do not correlate with the robustness of evoked responses. This methodology can be deployed directly to evaluate disease models for synaptic dysfunction and can be leveraged for drug development and precision medicine.

INTRODUCTION

Synapses are the major information-processing hubs in the brain. Synaptic dysfunction, or synaptopathy, is associated with a wide range of neurodevelopmental and neurodegenerative diseases, including intellectual disability, autism, Alzheimer's disease, Parkinson's disease, epilepsy, and many rare neurodevelopmental syndromes (Bridi and Hirth, 2018; Forero et al., 2006; Linda et al., 2018; Mandolesi et al., 2015; Zoghbi and Bear, 2012). The understanding and treatment of these conditions are hampered by the inaccessibility of the human brain and its synapses and by the fact that animal models often fail to recapitulate human brain disease phenotypes or predict treatment outcomes (Miller, 2010). Recent advances in induced pluripotent stem cell (iPSC) technology have overcome some of these difficulties by enabling the differentiation of human iPSCs into relatively pure populations of human neurons, generating unprecedented access to human neurons *in vitro* and providing new avenues to study human brain function and disease (Ichida and Kiskinis, 2015).

The authenticity of iPSC-derived models of human neurons has been documented using mRNA expression profiles and immunocytochemistry for cell identity, neuronal markers, morphology, and polarity. Furthermore, iPSC-derived human neurons exhibit action potential firing properties and spontaneous synaptic transmission (Bardy et al., 2016), and iPSC-derived neuronal models have been exploited to identify dysregulation of synaptogenesis or excitability (Farra et al., 2012; Mertens et al., 2015; Shcheglovitov et al., 2013). However, most currently available human cell models possess limited capacity to study synaptic transmission and plasticity. Synapses evolved to precisely couple the release of neurotransmitter to the arrival of action potentials on a millisecond timescale (Südhof, 2013) and can modulate the strength of their evoked responses within milliseconds up to minutes, depending on past experience or modulatory inputs. These short-lived changes in synaptic strength, or short-term plasticity (STP), are considered pivotal in the processing capacity of the brain (e.g., working memory) (Abbott and Regehr, 2004). Surprisingly few studies have tested evoked synaptic transmission in iPSC-derived human neurons, and no systematic studies of STP are available. Instead, studies addressing synaptic transmission or synaptopathies typically rely on spontaneous release only or on

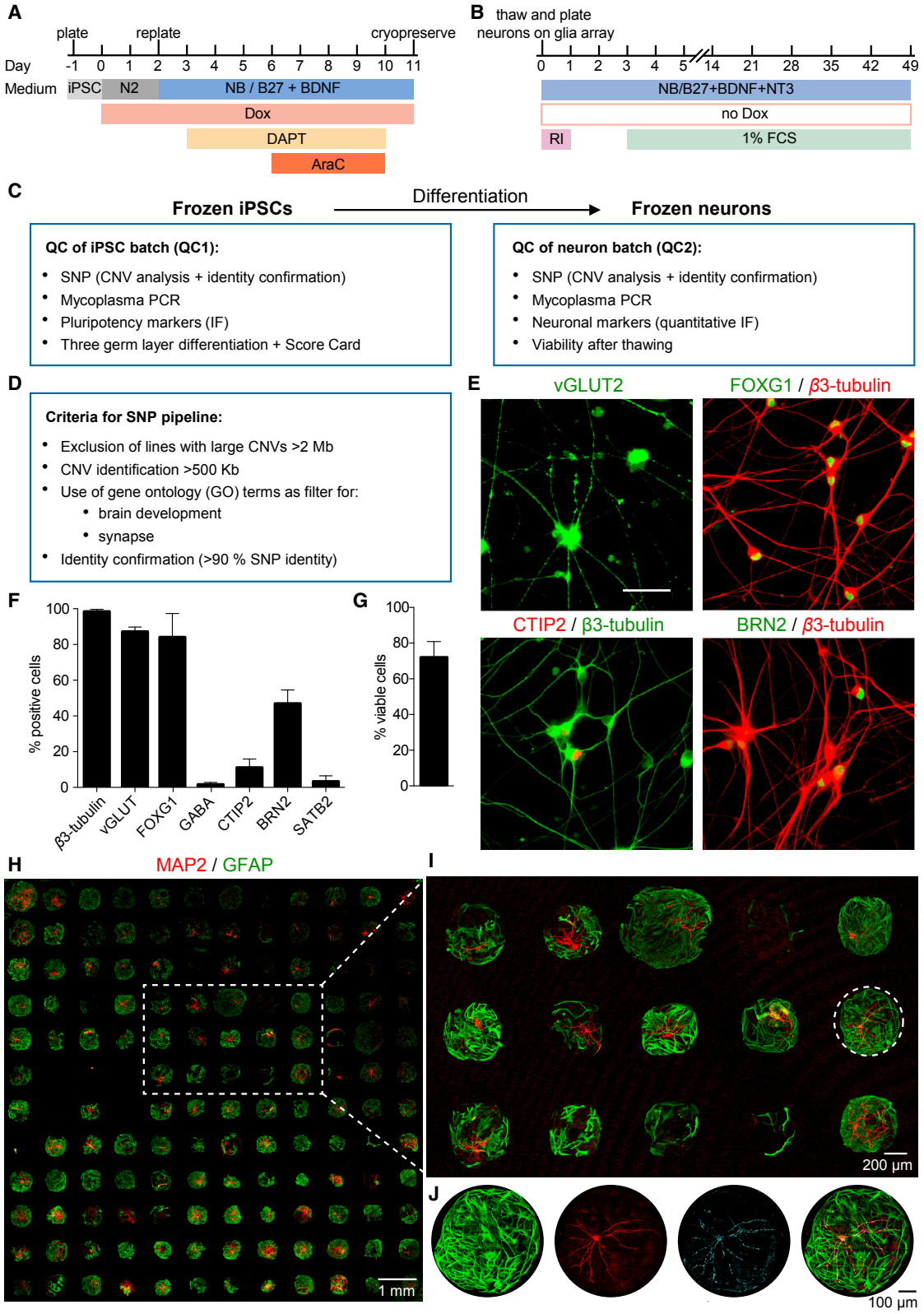

(legend on next page)

uncontrolled network activity (Shcheglovitov et al., 2013; Wang et al., 2016; Wen et al., 2014), with a few exceptions (Chanda et al., 2014; Shi et al., 2012b; Zhang et al., 2013).

The lack of robust, standardized models is a major limitation in modeling synaptic transmission in human neurons. Studying such processes requires the assessment of specific parameters, such as the number of release-ready vesicles (readily releasable pool [RRP]), their recruitment rate, and the energy barrier for fusion, that have been derived mostly from single neuron (autaptic) cultures in rodent studies. However, such standardized, reduced models are currently not available for human neurons. In this study, we have established such a human iPSC-derived model for the analysis of evoked synaptic transmission and STP.

We show that relevant parameters indicative of human synapse function can be assessed in a standardized and quantitative manner at single-cell resolution. We show that single human neurons, generated via different derivation methods, form mature synapses on glia microdot arrays and exhibit robust evoked synaptic transmission and STP. The current model provides all necessary parameters to systematically assess synaptic computation, also in relation to brain disorders (synaptopathies). Furthermore, these neuronal *in vitro* platforms are scalable for future drug development and precision medicine.

RESULTS

Generation of Single-Cell Human iPSC-Derived Neural Cultures on Micro-patterned Glia Arrays

To produce human excitatory neurons from pluripotent stem cells in a standardized and scalable manner, we adapted a forward programming approach that is based on forced expression of neurogenin 2 (NGN2) in PSCs (Zhang et al., 2013) and optimized this method to achieve a higher level of standardization. To this end, a doxycycline-inducible human *NGN2* expression cassette was targeted into both alleles of the AAVS1 "genomic safe harbor" locus of iPSCs, as shown before with mouse *Ngn2* (Wang et al., 2017) (Figure S1A). This strategy not only avoids random transgene integration and thus variable expression levels and insertional mutagenesis but also bypasses the risk for transgene silencing, which is otherwise often observed using lentiviral vectors (Qian et al., 2014). The resulting *NGN2*-transgenic iPSC clones are readily scalable without permanent antibiotic selection and allow the generation of large batches of iPSCs and NGN2 neurons. To ensure a complete and more synchronous conversion of iPSCs to NGN2 neurons, we included a transient application of DAPT, a γ-secretase inhibitor that blocks Notch signaling (Dovey et al., 2001). Although nearly all cells exhibited a neuronal morphology after 6 days, we applied the cytostatic drug cytosine arabinoside (AraC) for 4 days to eliminate any potentially remaining dividing cells, thereby obtaining a pure neuronal population within 11 days of doxycycline-mediated *NGN2* induction (Figure 1A). At this stage, NGN2 neurons were cryopreserved as large batches and subsequently thawed and plated on astrocyte microdot arrays for functional analysis (Figure 1B). See STAR Methods for further rationale behind these protocol changes.

Prior to downstream analysis, iPSCs and cryopreserved neurons were subjected to a stringent genomic quality control (QC) pipeline including SNP array-based copy number variation (CNV) analysis, combined with Gene Ontology (GO) term filter for brain development and synapse genes, and an identity confirmation (Figures 1C and 1D; Figures S1B–S1G). These QC criteria should ensure that only cell lines and batches free of additional CNVs affecting brain development and synapse-associated genes are used. Although we rarely observed large CNVs in control cell lines, we frequently identified newly acquired smaller CNVs affecting genes associated with brain development or synapse formation. This was the case in 23.5% of all batches (8 of 34) derived from control lines (12 different genomic backgrounds). Interestingly, in 5 of these cases, smaller CNVs comprised duplications of the ID1 and BCL2 genes on chromosome 20, a genomic adaption to cell culture frequently observed in iPSCs (Na et al., 2014). Further validation included marker expression. By quantification across multiple differentiations, we found that 99% of the cells expressed the pan-neuronal marker β3-tubulin, 87% the glutamatergic marker vGLUT2, and 84% the forebrain marker FOXG1, and only 1.6% of the cells stained positive for the inhibitory neurotransmitter GABA (Figures 1E and 1F). We also detected the cortical layer-specific markers CTIP2 (11%), BRN2 (47%), and SATB2 (3.4%) (Figures 1E and 1F; Figure S1D). The average post-thaw viability of NGN2 neurons was 72% (Figure 1G). Overall, this scalable protocol for the generation of cryopreserved batches of defined neuronal subtypes provides a high level of standardization for subsequent functional analysis.

For downstream functional analysis, we generated single-cell neuronal cultures, in which neurons grow in isolation on microdot

Figure 1. Generation and Validation of Cryopreserved NGN2 Neurons

(A) Timeline of the astrocyte-free protocol for the generation of NGN2 neurons.

(B) Timeline of the culture protocol for defrosted NGN2 neurons on astrocyte microdot arrays. RI, ROCK inhibitor.

(C) Overview of the quality control (QC) pipeline for batch validation of iPSCs and cryopreserved neurons, including CNV analysis with GO term filter, confirmation of genomic identity via SNP analysis of iPSCs and neurons, exclusion of mycoplasma contamination, assessment of cell viability, and quantitative immunofluorescence (IF) analysis to validate quality and purity of the different cell populations.

(D) Criteria for SNP pipeline.

(E) Immunostaining of the glutamatergic marker vGLUT2, the forebrain marker FOXG1, and the cortical layer-specific markers CTIP2 and BRN2 in NGN2 neurons generated from iPSCs from a healthy donor (C-14 m-s11) on day 18 of differentiation (day 7 after thawing). Scale bar, 50 μm.

(F) Quantification of neuronal and cortical marker expression of cryopreserved NGN2 neurons (n = 4).

(G) Post-thaw cell viability of NGN2 neurons (mean 72.2% ± 8.8% SD, n = 7).

(H) Stitched overview of astrocyte microdot coverslip containing human neurons.

(I) Zoom of section indicated in (H).

(J) Higher magnification image of the neuron indicated in (I), stained for GFAP, MAP2, and synaptophysin.

See also Figure S1.

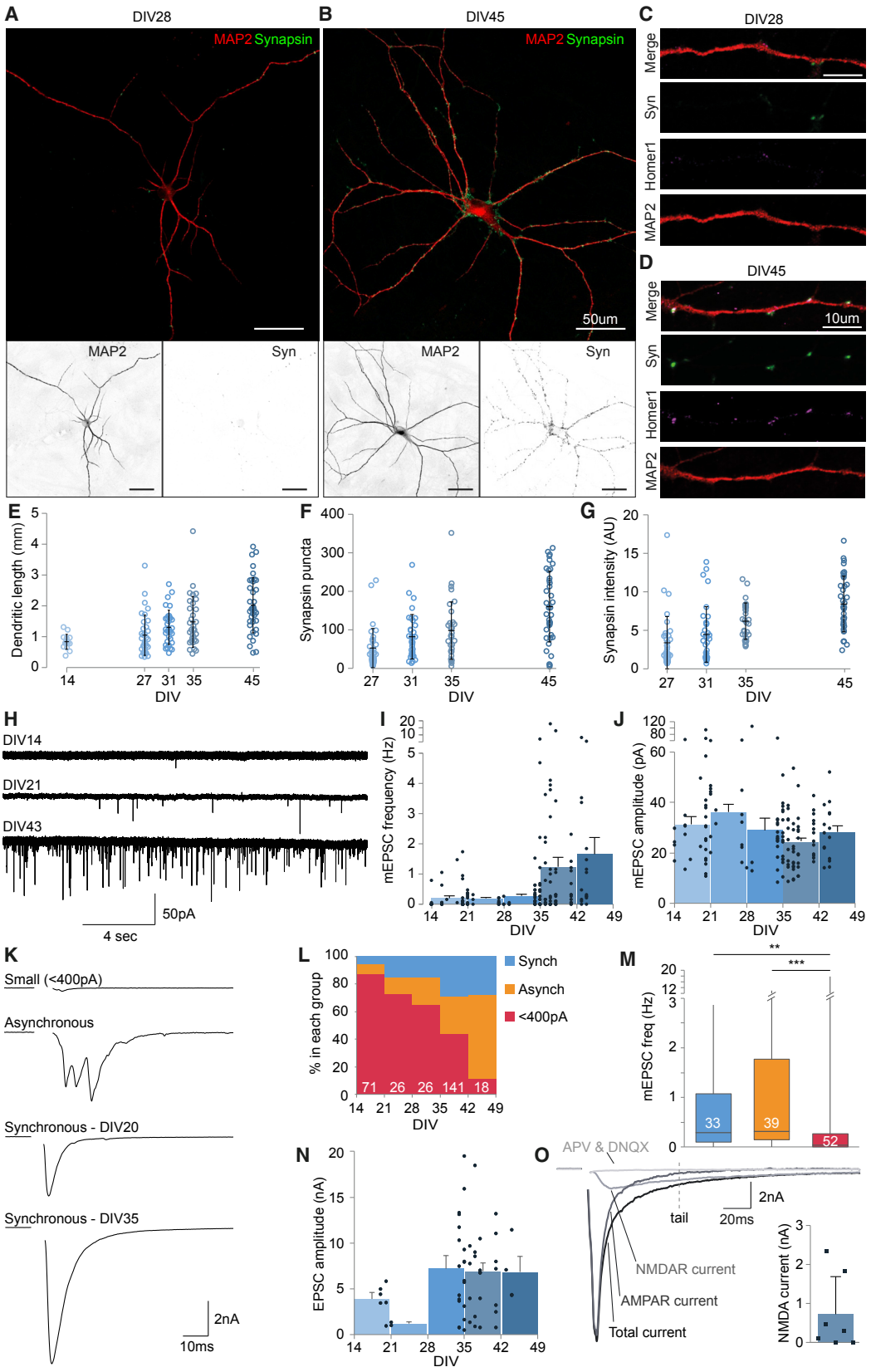

(legend on next page)

arrays of rat astrocytes (Figures 1H–1J). Astrocytes promote neuronal maturation and synaptic connectivity (Eroglu and Barres, 2010; Pfrieger, 2009), and in their absence, NGN2 neurons did not adhere to the microdots. When grown on preformed glia microdots, neurons make ample synapses onto themselves (autapses or autaptic cultures), which are functionally identical to regular synapses (Bekkers and Stevens, 1991). This culture system offers a standardized and restricted environment for neurons to develop. Evoked synaptic responses measured using a patch-clamp electrode in the soma report the average response of hundreds of synapses and can be used to quantify many synaptic parameters at single-cell level. In addition, structural and functional plasticity of the same synapse population can be reliably assessed. Furthermore, because the pre- and postsynaptic sides are part of the same cell, a single patch-clamp electrode suffices to both generate action potentials and record subsequent evoked synaptic current arriving at the soma. Finally, single-cell culture avoids potential pitfalls of network cultures such as heterogeneity in cell density, cellular identity, or survival. These are complicating factors for comparative studies. Taken together, this standardized *in vitro* approach allows the production of large batches of well-defined, cryopreserved human excitatory neurons that can be used for synaptic analyses at the single-cell level and for comparative functional studies using patch-clamp recording and other single-cell assays.

Single-Cell *NGN2*-Programmed Human Neurons Develop Functional Excitatory Synapses Capable of Evoked Synaptic Transmission

In standard low-density cultures, human NGN2 neurons have been shown to form functional synapses in less than 2 weeks (Zhang et al., 2013). We analyzed synapse formation after plating thawed NGN2 neurons on glia arrays (day *in vitro* [DIV] 0) and analyzed their morphological development up to DIV 45 using immunocytochemistry. Although human autapses rapidly developed a neuronal morphology, their dendritic length and synapse numbers remained relatively low after 2 weeks. Neurons continued to develop, and the mean number of synapses per neuron approached 200 at DIV 45 (Figures 2A–2F), which is within the range of mouse autapses (118–450 synapses per neuron; de Jong et al., 2016; Meijer et al., 2012; Schmitz et al., 2011, 2016; Toonen et al., 2006; Wierda et al., 2007). Concordantly, the intensity of synapse marker synapsin I in defined puncta increased up to DIV 45 (Figure 2G). At DIV 45, postsynaptic Homer1 puncta were opposing presynaptic synapsin puncta (Figures 2C and 2D). These findings indicate that NGN2 neurons tolerate cryopreservation and thawing, quickly adapt a neuronal morphology, and continue to form morphologically mature synapse patterns for at least 5 weeks.

To assess the functionality of these synapses, we analyzed synaptic transmission using whole-cell patch-clamp recordings with a single electrode to record from and deliver stimuli by brief somatic current injections. Most neurons (148 of 187) displayed spontaneous synaptic transmission in the absence of stimulation (Figure 2H). The frequency of these spontaneous events (miniature excitatory postsynaptic potentials [mEPSCs]) increased during maturation, while the amplitude was relatively stable from the developmental stage tested (DIV 14; Figures 2I and 2J). Morphological development of autaptic neurons is indistinguishable from neurons that develop in small micro-networks (Figures S2A–S2C). The presence of other neurons might slightly accelerate synapse formation, but spontaneous release is very similar after 3 weeks in culture (Figure S2D). Nonetheless, mEPSC frequency in human autaptic neurons was relatively low compared with mouse autaptic neurons (4–20 Hz; de Jong et al., 2016; Giniatullina et al., 2015; Groffen et al., 2010; He et al., 2017, 2018; Meijer et al., 2012, 2015, 2018; Schmitz et al., 2016). At 2 weeks in culture, the majority of neurons (>85%) did not produce a reliable evoked response to a single action potential stimulation (Figures 2K and 2L). During *in vitro* maturation, the percentage of responsive neurons increased to 56%–89% at 5–6 weeks in culture (91 of 159 cells with an EPSC $\geq$ 400 pA). Observed evoked responses were often not synchronous, leading to delayed multi-peak EPSCs (Figures 2K and 2L). Although mEPSC frequency was significantly higher in neurons that produced EPSCs > 400 pA, it was similar in neurons with synchronous and asynchronous evoked responses (Figure 2M). As a potential source of multi-peak EPSCs, the number of axons per neuron was investigated using ankyrin-G staining, a marker of the axon initial segment. Almost 30% of neurons had multiple axon initial segments after 6 weeks in culture (Figures S3A and S3B). Taken together, these data show that synaptic transmission gradually developed in single neurons on glia islands, initially with merely spontaneous events and subsequently with action potential evoked EPSCs. The spontaneous event frequency did not correlate with the ability of synapses to synchronize their evoked responses.

To test the development of synchronous evoked responses systematically during development, only neurons with synchronized EPSCs were included and plotted against their time in

Figure 2. Induced Human Glutamatergic Forebrain Neurons Develop Mature Synapses

(A and B) Typical examples of confocal images from single-cell NGN2 neurons at (A) DIV 28 and (B) DIV 45. Scale bar, 50 μm.

(C and D) Zoom of dendritic stretch at (C) DIV 28 and (D) DIV 45. Scale bar, 10 μm.

(E–G) Quantification of (E) dendritic length, (F) number of synapsin puncta, and (G) average intensity of synapsin puncta over time (mean ± SD, N = 3 cultures).

(H) Typical examples of spontaneous release of single vesicles at DIV 14, 21, and 43.

(I and J) Quantification of (I) frequency (n = 187 neurons) and (J) amplitude (n = 148 neurons) of spontaneous mEPSCs over time (mean ± SEM, N = 9 cultures).

(K) Typical examples of action potential-evoked release in NGN2 neurons.

(L) Percentage of evoked responses falling in the categories "synchronous EPSC," "asynchronous EPSC," and "EPSC < 400 pA" during development.

(M) Boxplot of spontaneous release frequency in neurons categorized on the basis of their evoked responses as in (L).

(N) Quantification of synchronous EPSC amplitude during development (mean ± SEM, n = 56 neurons, N = 8 cultures).

(O) Typical example of EPSC consisting of AMPA- and NMDA-dependent currents. Quantification of peak tail current 70 ms after action potential induction (mean ± SD, n = 7).

See also Figures S2 and S3.

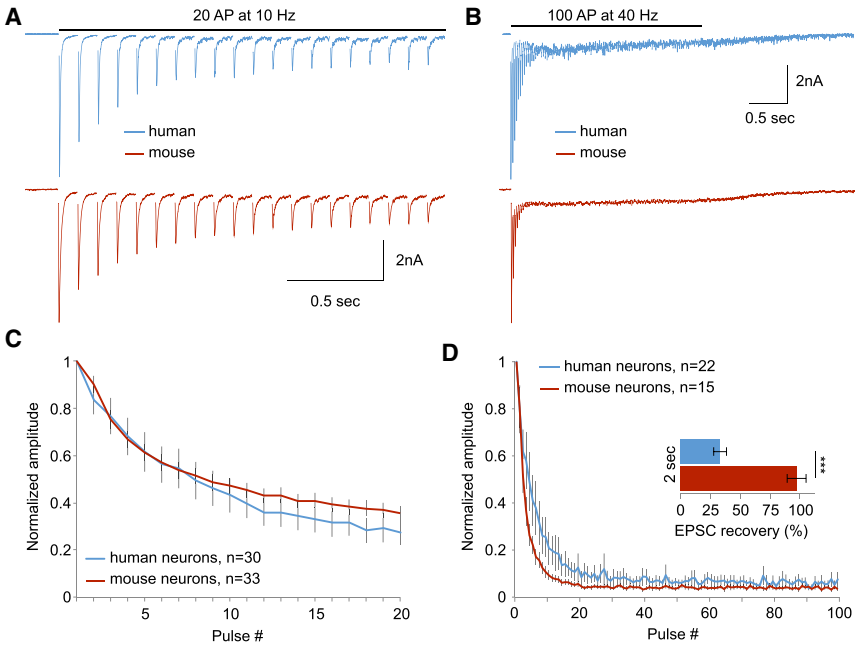

Figure 3. Single Human NGN2 Neurons Show Synaptic Depression in Response to Repetitive Stimulation

(A and B) Typical examples of evoked responses to a stimulation train in NGN2 neurons and *munc18-1* null mouse neurons in which wild-type Munc18-1 was reintroduced using lentiviral expression, resulting in wild-type synaptic transmission. Stimulation trains consisted of (A) 20 pulses given at 10 Hz and (B) 100 pulses given at 40 Hz.

(C) Normalized EPSC amplitude during 10 Hz stimulation train.

(D) Normalized EPSC amplitude during 40 Hz stimulation train. Inset shows recovery of the EPSC amplitude two seconds after the end of stimulation as percentage of the initial EPSC at the start of stimulation (human: 33.2% ± 5.4%, n = 22; mouse: 97.3% ± 7.9%, n = 15; ***p < 0.0001, t test). Neurons were recorded at DIV 20–44 (human) and DIV 13–18 (mouse). Data are represented as mean ± SEM.

culture (Figure 2N). In young neurons, synchronous EPSCs were smaller compared with those in older neurons but were stable at DIV 34–44, with amplitudes up to 20 nA. Resting membrane potentials (RMPs) were also stable during this period (Figure S3C; for a thorough analysis of active and passive membrane properties of NGN2 neurons, see accompanying paper from Rhee et al., 2019 in this issue of *Cell Reports*). Hence, during *in vitro* maturation, single neurons on glia islands have developed synchronous evoked responses within 3 weeks in culture, but the incidence of these synchronous evoked responses drastically increases with prolonged maturation. In 5-week-old neurons recorded in Mg^{2+}-free medium, ~70% of evoked responses were composed of AMPA- and NMDA-dependent currents (five of seven cells). Because of the faster kinetics of AMPA-dependent currents, the tail current was used to estimate the NMDA-dependent component (Figure 2O, inset). Although the evoked current in the tail is composed almost entirely of NMDA-dependent current, it will underestimate the peak NMDA current. In two cells, DNQX was added to delineate the NMDA-dependent current (Figure 2O), resulting in an average NMDA current of 1.1 nA. These results confirm that mature postsynaptic responses have developed in these neurons. Overall, these results show that excitatory autaptic human neurons develop mature evoked synaptic transmission on glia microdot arrays within 5 weeks.

Cultured Human Excitatory Synapses Show STP

Human synapses show different forms of modulation, including STP (Testa-Silva et al., 2014). To assess whether NGN2 neurons also express this type of synaptic modulation, autaptic human neurons were subjected to train stimulation at 10 or 40 Hz (Figures 3A and 3B). Human NGN2 neurons showed strong depression of their EPSC amplitude during sustained stimulation at 10 Hz (Figure 3C). On average, EPSC amplitude depressed at similar rates compared with control mouse neurons (Figure 3C). During more intense stimulation, human neurons showed slightly slower depression (Figure 3D), with a larger diversity in rundown patterns. Stimulation at 40 Hz depletes the pool of readily releasable vesicles, as vesicle exocytosis is faster than vesicle recruitment and EPSC amplitudes diminish. After stimulation, vesicle recruitment quickly refills the vesicle pool. Mouse synapses recovered their initial full EPSC amplitude within 2 s, but human synapses recovered to only one third of the initial EPSC amplitude during this period (Figure 3D, inset), whereas the full EPSC amplitude had recovered after 1 min (93% ± 7.6%, n = 22). These results show that human NGN2 neurons show robust synaptic strength modulation, similar to mouse neurons, but differ in recovery kinetics after intense stimulation.

STP Replicates among Human Autaptic NGN2 Neurons Derived from Different Backgrounds

To assess the reproducibility of the single neuron assay, human NGN2 neurons were generated from iPSC lines from two different (healthy) donors (C14m and C35m, both adult men) and analyzed in parallel cultures. Both lines followed similar developmental patterns (dendritic growth, synapse development; Figures S4A–S4C). C14m neurons showed a trend toward larger EPSC amplitude (Figure S4D), and higher paired pulse ratios (Figures S4E and S4F). Both the amplitude and frequency of spontaneous release were higher in C14m neurons (Figures S4G and S4H), but synapses derived from both healthy donors showed similar STP upon 10 or 40 Hz stimulation (Figure 4). The rate of EPSC depression might be slightly stronger in C35m neurons, especially during 40 Hz stimulation. Both groups recovered their EPSC sizes to a similar extent within 2 s after stimulation and fully within 60 s (Figure 4D, inset). These results suggest that several basic parameters of synaptic transmission are different in human neurons derived from two healthy donors, but STP kinetics and extent were similar. Thus, autaptic cultures of single human neurons are a suitable model to study synapse strength modulation.

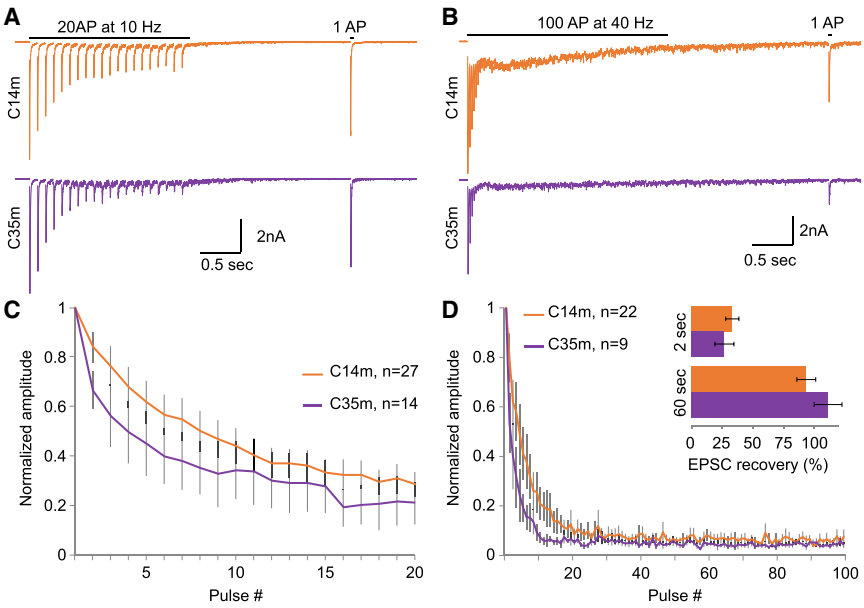

Figure 4. Robust Synaptic Computation in Different Genetic Backgrounds

(A and B) Typical examples of evoked responses in human NGN2 neurons generated from iPSCs from two healthy donors (C-14 m-s11 and C-35 m-r1) in response to a stimulation train of (A) 20 pulses given at 10 Hz and (B) 100 pulses given at 40 Hz followed by a recovery pulse after 2 s.

(C) Normalized EPSC amplitude during 10 Hz stimulation.

(D) Normalized EPSC amplitude during 40 Hz stimulation. Inset shows recovery of the EPSC amplitude two seconds after the end of 40 Hz train as percentage of the initial EPSC. Neurons were recorded at DIV 34–44. Data are represented as mean ± SEM (N = 3 parallel cultures).

See also Figure S4.

Synaptic Transmission in Classically Derived Inhibitory Neurons Is Stable between 8 and 12 Weeks in Culture

To test whether this single-cell model not only works with glutamatergic NGN2 neurons but is applicable to a large variety of human neurons and differentiation protocols, we generated inhibitory forebrain neurons using a classical *in vitro* differentiation protocol. These single GABAergic neurons were first assessed on their morphological development. Dendritic length and synaptophysin puncta increased over time, with a striking jump between 6 and 8 weeks in culture (Figures 5A and 5B). At earlier time points, neurons showed growth cones (Figure 5A, arrow) but little synaptic puncta. To confirm their GABAergic identity, immunostainings were performed for VGAT and Neuroligin2, a cell adhesion protein localized to the postsynaptic density of inhibitory neurons (Varoqueaux et al., 2004). VGAT and Neuroligin2 puncta also increased over time and were found to co-localize (Figures 5C–5E). These data suggest that both the presynaptic and postsynaptic aspects of GABAergic synapses develop between 6 and 8 weeks in single-neuron cultures of human classic GABA neurons (Figures 5C–5E).

Synapse physiology was performed at 8, 10, or 12 weeks in culture. During this time, miniature inhibitory postsynaptic current (mIPSC) frequency and amplitude were stable (Figures 6A–6C). Approximately 40% of the neurons generated a synchronous IPSC upon single depolarization, while 45% did not and 13% produced IPSCs containing multiple peaks. The IPSC size was on average 1 nA (1.04 ± 0.16 nA, n = 28) and was stable over time (Figure 6D). Inhibitory neurons display short-term depression, just as excitatory neurons, albeit with faster kinetics. Human GABAergic autapses were stimulated with eight pulses at 10 Hz, followed by a recovery pulse after 400 ms, which led to rapid depression of IPSC amplitude (Figure 6E). IPSC size recovered from depression to ~20% of their initial IPSC within 400 ms (Figure 6E, inset).

Because longer culture times were required for GABAergic neurons generated via classical *in vitro* differentiation (8–12 weeks' versus 5–6 weeks' maturation), we tested whether increasing glial support achieved by placing the microdot glia arrays in close proximity to a glia feeder layer (sandwich culture) would promote synaptic transmission and plasticity (Kaech and Banker, 2006). We found no systematic added benefit in terms of IPSC amplitude, paired pulse ratio, or morphological development (Figures 6F and 6G; Figure S5). These results show that also human GABAergic neurons grown on glia microdot arrays show evoked synaptic transmission and STP and can be used as a disease model for dysfunction of GABAergic synapses.

DISCUSSION

We describe here a standardized approach to assess synapse physiology with single-cell resolution in iPSC-derived human neurons cultured on glia microdot arrays for the comparative analysis of synaptic computation in cryopreserved neurons derived from human somatic tissue. This methodology can be applied to a variety of differentiation approaches (both classical and forward programming) and neuronal cell types and supports functional neurons for at least 12 weeks *in vitro*. Synaptic genes and protein networks are implicated in neuropsychiatric disorders (De Rubeis et al., 2014; Fromer et al., 2014; Gai et al., 2012; Sanders et al., 2015) and rare disease variants in synaptic genes are found in a range of neurodevelopmental disorders (Baker et al., 2015; Lipstein et al., 2017; Schubert et al., 2014; Shen et al., 2014; Stamberger et al., 2016; Tarpey et al., 2009; von Spiczak et al., 2017). We are confident that the methodology presented here facilitates the study of these disorders using patient-derived single neurons.

To base all functional analyses on a standardized cellular model, we used a transcription factor-mediated forward programming approach enabling rapid derivation of neurons and thus minimizing experimental variation caused by extended culture periods required in conventional extrinsic factor-driven protocols (Shi et al., 2012a). Furthermore, the use of viruses for

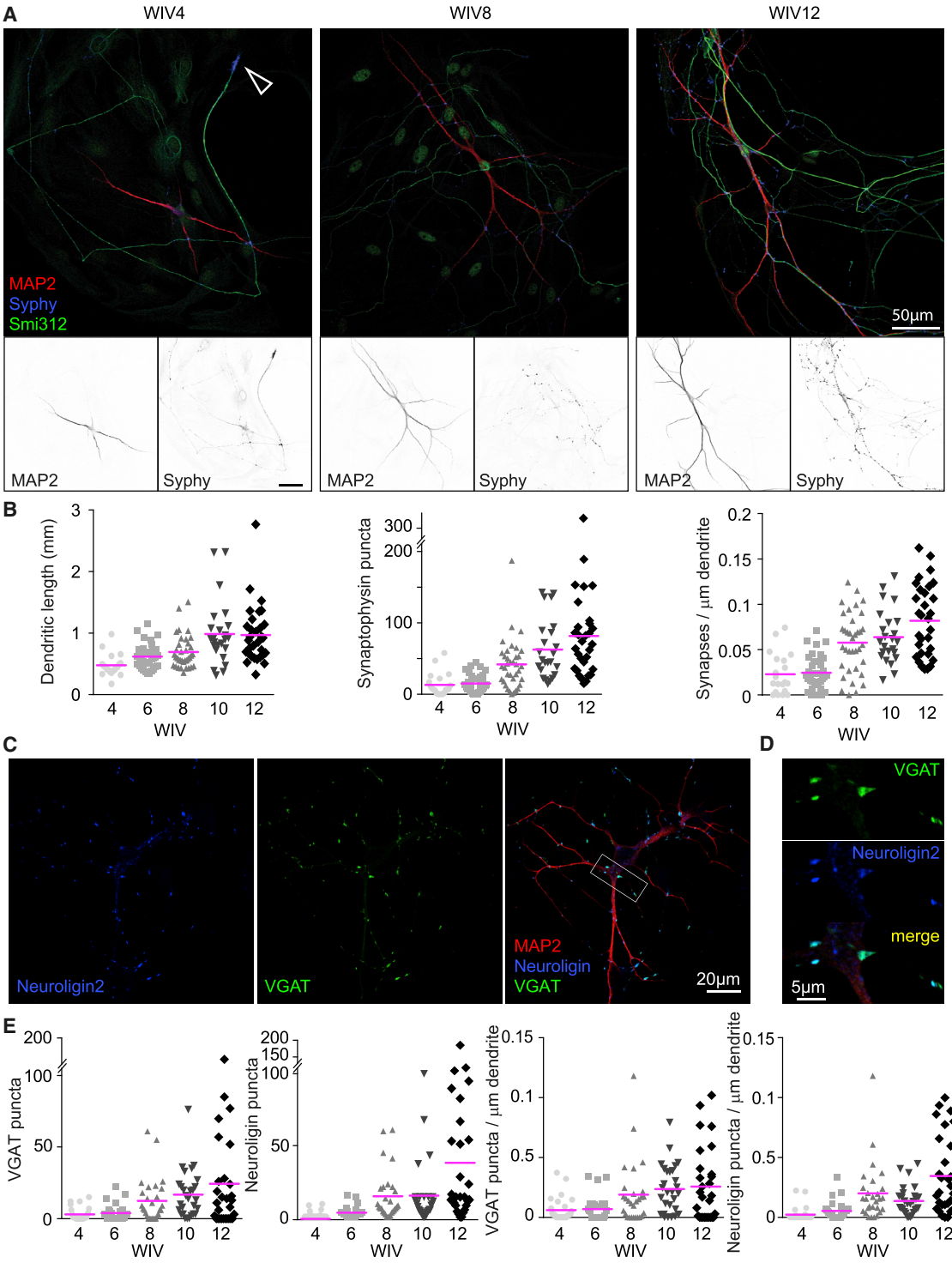

Figure 5. Classically Differentiated GABAergic Forebrain Neurons Also Develop on Single-Cell Rat Microdot Arrays, Albeit on a Longer Timescale

(A) Typical examples of classic GABAergic forebrain neurons after 4, 8, and 12 weeks *in vitro* (WIV). Open arrowhead points at growth cone.

(B) Quantification of dendritic length, synaptophysin puncta, and synaptic density over time. Bars represent mean.

(C) Typical example of a confocal image of an inhibitory neuron after 12 weeks in culture.

(D) Zoom of section in (C) showing overlap between VGAT and neuroligin staining.

(E) Quantification of VGAT and neuroligin puncta and density per dendritic stretch. Bars represent mean.

See also Figure S5.

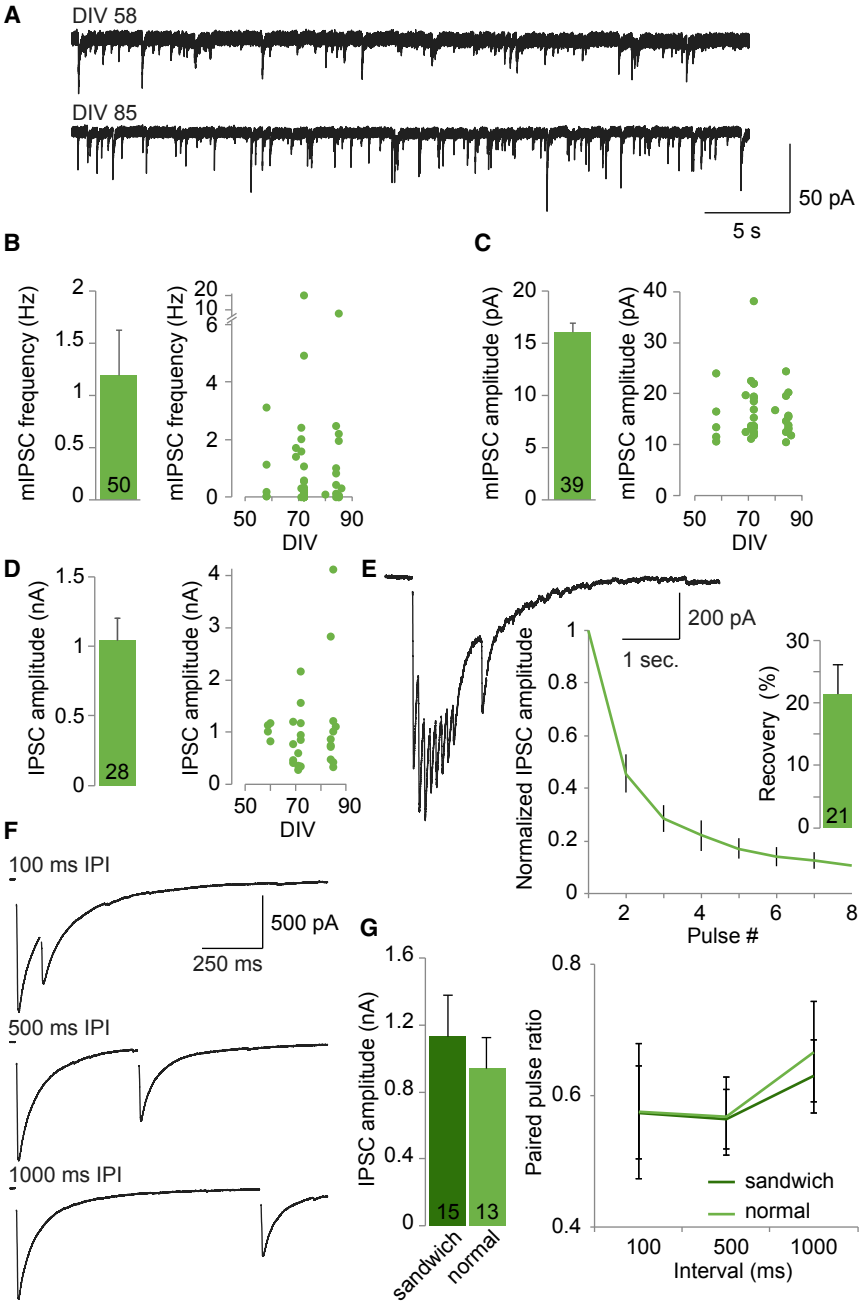

Figure 6. Classic GABA Neurons Show Stable Synaptic Transmission and Computation between 8 and 12 Weeks in Culture

(A) Typical examples of spontaneous release in classically differentiated inhibitory neurons after 58 or 85 days in culture.

(B and C) Quantification of frequency (B) and amplitude (C) of spontaneous mIPSCs.

(D) Quantification of IPSC amplitude measured at different days *in vitro* (DIV).

(E) Typical example of synaptic response to eight pulses at 10 Hz followed by a recovery pulse after 400 ms, with quantification of IPSC depression during stimulation (IPSC amplitude normalized to initial response at start train). Inset shows quantification of recovery from depression (IPSC amplitude of recovery pulse as percentage of initial response at start train).

(F) Typical examples of paired pulse plasticity in inhibitory human neurons.

(G) Quantification of IPSC amplitude and paired pulse ratio in neurons grown on coverslips that were in sandwich culture with a glia feeder layer compared with those that were not. Data are represented as mean ± SEM (n = number of neurons, N = 4 cultures).

transgene delivery was bypassed to avoid heterogeneous expression levels, insertional mutagenesis, and premature transgene silencing. Targeting transgenic *NGN2* into the *AAVS1* safe harbor locus ensures that each cell carries the same copy number at the same genomic site, and clonal *NGN2*-transgenic iPSC lines are readily scalable for bulk production of neurons. Although the safe harbor strategy has been used for neuronal conversion of iPSCs also by others (Pawlowski et al., 2017; Wang et al., 2017), we streamlined the neuronal derivation process by the application of compounds that accelerate and synchronize entry into a post-mitotic neuronal state and eliminate potentially remaining dividing cells. These measures allowed us to generate pure neuronal cultures within 11 days that are amenable to cryopreservation in large batches with high post-thaw recovery rates. Combined with stringent QC standards including high-resolution SNP analyses to exclude batches with culture-induced genomic CNVs, this neuronal derivation pipeline represents a highly standardized and controlled platform for functional analyses.

Using this pipeline, we show that excitatory NGN2 neurons indeed show a neuronal morphology, express synaptic markers, and form functional synapses with robust evoked synaptic responses in 60% of the neurons after 5 weeks in culture. Previous studies using traditional (mass) cultures of *Ngn2*-programmed neurons have reported that synaptic responses can be evoked at 2–3 weeks in culture (Zhang et al., 2013). The data presented here indicate that extending the culture period for NGN2 neurons to 5 weeks leads to synaptically more mature neurons. In addition, the single-neuron cultures presented here allow the assessment of important synaptic parameters for structural plasticity (synapses per neuron) and functional plasticity (paired pulse plasticity, synaptic depression, and synaptic recovery). Previous studies also showed that NMDAR-mediated currents are mostly extra-synaptic in *Ngn2*-programmed neurons (Nehme et al., 2018). However, prolonged culture as single neurons yields NGN2 neurons that display

robust synaptic NMDAR-mediated currents (Figure 2O). The observation of a subpopulation with multiple axons is striking (Figure S3) but not unique to iPSC-derived neurons. Primary neurons can also have multiple axon initial segments (AISs) (Guo et al., 2017; Huang and Rasband, 2018), which are electrically active and result in normal action potential initiation, leading us to conclude that NGN2 neurons are nevertheless functional. Taken together, single-cell cultures of *NGN2*-programmed excitatory neurons provide a robust and standardized model to study synapse function, with unique opportunities that cannot be assessed with existing *in vitro* models.

Many studies of human neurons present miniature (spontaneous) synaptic responses as evidence for synaptic maturation of human neuron cultures. In fact, a large fraction of published studies report spontaneous synaptic responses without demonstrating evoked synaptic transmission. Certain synaptic phenotypes, such as a reduction in the number of synapses or postsynaptic changes, can be readily uncovered using spontaneous release. However, we show here that spontaneous synaptic responses are a poor predictor of synaptic maturity, and their frequency does not correlate with the synchronicity of evoked synaptic transmission. Hence, for studies investigating synaptic development and function in human neurons, it is important to base conclusions on the analysis of evoked responses, not on spontaneous synaptic responses only.

Despite a high degree of methodological standardization, human neurons display substantial heterogeneity in their synaptic responses. This may in part reflect the diversity in synaptic properties among neurons in the CNS (Dittman et al., 2000), but differences in maturation and/or growth parameters among neurons also contribute. Synapse numbers tend to correlate with dendritic complexity and will affect spontaneous release and evoked response size (but not STP, release probability, and synaptic recovery). Synaptic transmission and plasticity are complex phenomena to which many genes or proteins contribute. Consequently, the unique genomic background of every control or patient line is expected to contribute many specific modifying factors that influence these phenomena and produce diversity in responses. Characterizing the broad range of genetic factors that could influence synapse function will be critical for our understanding of the influence of genomic background, especially if effects of a mutation or CNV are multifactorial.

Although certain synaptic parameters (paired-pulse plasticity, synaptic recovery) were similar between neurons derived from two different healthy adult men, we observed differences in spontaneous release amplitude and frequency (Figure S4). A change in mEPSC amplitude suggests postsynaptic changes such as a reduction or increase in receptor number or density, while a change in the mEPSC frequency can result from a change in the number of active synapses. These differences were observed in all three independent cultures, demonstrating the sensitivity and stability of the assay but also underscoring the need for isogenic controls in future studies on synaptic transmission and plasticity, because the use of unrelated controls provides a substantial potential source of confounding effects.

Glutamatergic synapse development and function is largely unaffected by the presence of neighboring neurons or their activity, and autapses have been shown to behave similarly in many respects to synapses formed between neurons (Bekkers and Stevens, 1991; Chang et al., 2014; Harms et al., 2005; Mennerick et al., 1995). Indeed, we find that morphological development in NGN2 neurons was very similar in single-cell and micro-network cultures, as was the rate of spontaneous release (Figure S2). We did not extend the functional analysis further, because other synaptic parameters are very difficult to obtain from network cultures (synaptic plasticity, release probability, pool size, etc.).

A consistent feature in both NGN2 neuron control lines was the slow recovery from synaptic depression (Figure 4D). In contrast, human synapses in surgically removed brain tissue recover more rapidly from depression than rodent synapses, suggesting a larger information transfer capacity (Testa-Silva et al., 2014). The slower recovery in iPSC-derived neurons might therefore not model human neuron properties accurately. Incomplete maturation (Nehme et al., 2018) or insufficient support during extended culture periods may contribute to this. On the other hand, information on human synapse physiology is still scarce and naturally based on limited resources. Different synapses in the human brain at different ages most likely have diverse properties. Hence, a systematic future comparisons of synapse properties between specific population of synapses in primary human neurons and from iPSC-derived neurons are required to address how the latter can optimally model the former regarding the recovery from synaptic depression.

Changes in synaptic strength dependent on the (recent) past activity are a powerful way to alter network properties (e.g., for spatial navigation, feature extraction, or sound localization) and are widely accepted to be at the basis of the brain's computational power (Abbott and Regehr, 2004). Human synapses show several of such changes in strength, such as spike timing-dependent plasticity (Testa-Silva et al., 2010), long-term depression (LTD) or long-term potentiation (LTP) (Beck et al., 2000; Chen et al., 1996), and short-term depression (STD) (Testa-Silva et al., 2014), similar to previous observations in rodents. Here we show that iPSC-derived human cell models can be generated that display synaptic plasticity features such as synaptic facilitation, depression, and rebound after depression. Such a standardized single-cell method to study human synaptic transmission and plasticity will facilitate studies of synaptic dysfunction in human brain disorders and also on the patient's own genomic background.

STAR★METHODS

Detailed methods are provided in the online version of this paper and include the following:

- KEY RESOURCES TABLE
- CONTACT FOR REAGENT AND RESOURCE SHARING
- EXPERIMENTAL MODEL AND SUBJECT DETAILS
  - Laboratory Animals
  - iPSC lines
- METHOD DETAILS
  - Plasmid cloning
  - AAVS1 targeting
  - Forward programming into glutamatergic neurons
  - Differentiation into GABAergic forebrain neurons

- Quality control
- SNP analysis and CNV calling
- Microdot arrays
- Primary Mouse Neuron Culture
- Thawing and culture of cryopreserved human neurons
- Morphological analysis
- Synapse physiology

● QUANTIFICATION AND STATISTICAL ANALYSIS

SUPPLEMENTAL INFORMATION

Supplemental Information can be found online at https://doi.org/10.1016/j.celrep.2019.04.058.

ACKNOWLEDGMENTS

We thank Vincent Huson and Jurjen Broeke for developing scripts to analyze the physiological data and Frank den Oudsten for producing glia microdot arrays. We acknowledge Sven Stringer and Josefin Werme for expert help with identifying copy number variants from SNP arrays. We thank Dr. Su-Chun Zhang for kindly providing the AAVS targeting vector and corresponding TALEN plasmids. We gratefully acknowledge the technical support of Tamara Bechler. The research leading to these results has received funding from COSYN (Comorbidity and Synapse Biology in Clinically Overlapping Psychiatric Disorders; to M.V., P.F.S., and O.B.) (Horizon 2020 Program of the European Union under RIA grant agreement 667301); a European Research Council (ERC) advanced grant (322966) of the European Union (to M.V.), and the German Federal Ministry of Education and Research (BMBF) within the framework of the e:Med research and funding concept (grant 01ZX1314A-IntegraMent to O.B.).

AUTHOR CONTRIBUTIONS

M.V., O.B., and P.F.S. conceptualized the project. The neuronal derivation pipeline was developed by K.R., including QC and cryopreservation. T.K. and M.H. established the NGN2 system under the supervision of M.P. D.S. established single-cell human neurons cultures. M.M. conducted, analyzed, interpreted, and supervised physiology experiments. J.W.B., J.A.C., H.C.A.L., and L.A.v.L. conducted physiology experiments and analyzed data. J.W.B. and D.S. performed and analyzed single-cell neuronal morphology. M.V., R.F.T., and L.N.C. supervised structural and functional analysis of single-cell human neurons. O.B. and M.P. supervised the neuronal derivation pipeline. M.M. and M.V. wrote the manuscript with input from all authors.

DECLARATION OF INTERESTS

O.B. is a co-founder of and has stock in Life & Brain GmbH.

Received: October 8, 2018
Revised: February 5, 2019
Accepted: April 10, 2019
Published: May 14, 2019

REFERENCES

Abbott, L.F., and Regehr, W.G. (2004). Synaptic computation. Nature *431*, 796–803.

Baker, K., Gordon, S.L., Grozeva, D., van Kogelenberg, M., Roberts, N.Y., Pike, M., Blair, E., Hurles, M.E., Chong, W.K., Baldeweg, T., et al. (2015). Identification of a human synaptotagmin-1 mutation that perturbs synaptic vesicle cycling. J. Clin. Invest. *125*, 1670–1678.

Bardy, C., van den Hurk, M., Kakaradov, B., Erwin, J.A., Jaeger, B.N., Hernandez, R.V., Eames, T., Paucar, A.A., Gorris, M., Marchand, C., et al. (2016). Predicting the functional states of human iPSC-derived neurons with single-cell RNA-seq and electrophysiology. Mol. Psychiatry *21*, 1573–1588.

Beck, H., Goussakov, I.V., Lie, A., Helmstaedter, C., and Elger, C.E. (2000). Synaptic plasticity in the human dentate gyrus. J. Neurosci. *20*, 7080–7086.

Bekkers, J.M., and Stevens, C.F. (1991). Excitatory and inhibitory autaptic currents in isolated hippocampal neurons maintained in cell culture. Proc. Natl. Acad. Sci. U S A *88*, 7834–7838.

Bertalan, M. (2017). IPSYCHCNV: A robust method for copy number variation detection on dried blood spots. Eur. Neuropsychopharmacol. *27*, 163.

Bridi, J.C., and Hirth, F. (2018). Mechanisms of α-synuclein induced synaptopathy in Parkinson's disease. Front. Neurosci. *12*, 80.

Chanda, S., Ang, C.E., Davila, J., Pak, C., Mall, M., Lee, Q.Y., Ahlenius, H., Jung, S.W., Südhof, T.C., and Wernig, M. (2014). Generation of induced neuronal cells by the single reprogramming factor ASCL1. Stem Cell Reports *3*, 282–296.

Chang, C.L., Trimbuch, T., Chao, H.T., Jordan, J.C., Herman, M.A., and Rosenmund, C. (2014). Investigation of synapse formation and function in a glutamatergic-GABAergic two-neuron microcircuit. J. Neurosci. *34*, 855–868.

Chang, C.C., Chow, C.C., Tellier, L.C., Vattikuti, S., Purcell, S.M., and Lee, J.J. (2015). Second-generation PLINK: rising to the challenge of larger and richer datasets. Gigascience *4*, 7.

Chen, W.R., Lee, S., Kato, K., Spencer, D.D., Shepherd, G.M., and Williamson, A. (1996). Long-term modifications of synaptic efficacy in the human inferior and middle temporal cortex. Proc. Natl. Acad. Sci. U S A *93*, 8011–8015.

de Jong, A.P., Meijer, M., Saarloos, I., Cornelisse, L.N., Toonen, R.F., Sørensen, J.B., and Verhage, M. (2016). Phosphorylation of synaptotagmin-1 controls a post-priming step in PKC-dependent presynaptic plasticity. Proc. Natl. Acad. Sci. U S A *113*, 5095–5100.

De Rubeis, S., He, X., Goldberg, A.P., Poultney, C.S., Samocha, K., Cicek, A.E., Kou, Y., Liu, L., Fromer, M., Walker, S., et al.; DDD Study; Homozygosity Mapping Collaborative for Autism; UK10K Consortium (2014). Synaptic, transcriptional and chromatin genes disrupted in autism. Nature *515*, 209–215.

Dittman, J.S., Kreitzer, A.C., and Regehr, W.G. (2000). Interplay between facilitation, depression, and residual calcium at three presynaptic terminals. J. Neurosci. *20*, 1374–1385.

Dovey, H.F., John, V., Anderson, J.P., Chen, L.Z., de Saint Andrieu, P., Fang, L.Y., Freedman, S.B., Folmer, B., Goldbach, E., Holsztynska, E.J., et al. (2001). Functional gamma-secretase inhibitors reduce beta-amyloid peptide levels in brain. J. Neurochem. *76*, 173–181.

Eroglu, C., and Barres, B.A. (2010). Regulation of synaptic connectivity by glia. Nature *468*, 223–231.

Farra, N., Zhang, W.B., Pasceri, P., Eubanks, J.H., Salter, M.W., and Ellis, J. (2012). Rett syndrome induced pluripotent stem cell-derived neurons reveal novel neurophysiological alterations. Mol. Psychiatry *17*, 1261–1271.

Forero, D.A., Casadesus, G., Perry, G., and Arboleda, H. (2006). Synaptic dysfunction and oxidative stress in Alzheimer's disease: emerging mechanisms. J. Cell. Mol. Med. *10*, 796–805.

Fromer, M., Pocklington, A.J., Kavanagh, D.H., Williams, H.J., Dwyer, S., Gormley, P., Georgieva, L., Rees, E., Palta, P., Ruderfer, D.M., et al. (2014). De novo mutations in schizophrenia implicate synaptic networks. Nature *506*, 179–184.

Gai, X., Xie, H.M., Perin, J.C., Takahashi, N., Murphy, K., Wenocur, A.S., D'arcy, M., O'Hara, R.J., Goldmuntz, E., Grice, D.E., et al. (2012). Rare structural variation of synapse and neurotransmission genes in autism. Mol. Psychiatry *17*, 402–411.

Giniatullina, A., Maroteaux, G., Geerts, C.J., Koopmans, B., Loos, M., Klaassen, R., Chen, N., van der Schors, R.C., van Nierop, P., Li, K.W., et al. (2015). Functional characterization of the PCLO p.Ser4814Ala variant associated with major depressive disorder reveals cellular but not behavioral differences. Neuroscience *300*, 518–538.

Groffen, A.J., Martens, S., Díez Arazola, R., Cornelisse, L.N., Lozovaya, N., de Jong, A.P., Goriounova, N.A., Habets, R.L., Takai, Y., Borst, J.G., et al. (2010). Doc2b is a high-affinity Ca2+ sensor for spontaneous neurotransmitter release. Science *327*, 1614–1618.

Guo, Y., Liu, Z., Chen, Y.K., Chai, Z., Zhou, C., and Zhang, Y. (2017). Neurons with multiple axons have functional axon initial segments. Neurosci. Bull. *33*, 641–652.

Harms, K.J., Tovar, K.R., and Craig, A.M. (2005). Synapse-specific regulation of AMPA receptor subunit composition by activity. J. Neurosci. *25*, 6379–6388.

He, E., Wierda, K., van Westen, R., Broeke, J.H., Toonen, R.F., Cornelisse, L.N., and Verhage, M. (2017). Munc13-1 and Munc18-1 together prevent NSF-dependent de-priming of synaptic vesicles. Nat. Commun. *8*, 15915.

He, E., Lozano, M.A.G., Stringer, S., Watanabe, K., Sakamoto, K., den Oudsten, F., Koopmans, F., Giamberardino, S.N., Hammerschlag, A., Cornelisse, L.N., et al. (2018). MIR137 schizophrenia-associated locus controls synaptic function by regulating synaptogenesis, synapse maturation and synaptic transmission. Hum. Mol. Genet. *27*, 1879–1891.

Hosaka, M., and Südhof, T.C. (1999). Homo- and heterodimerization of synapsins. J. Biol. Chem. *274*, 16747–16753.

Huang, C.Y., and Rasband, M.N. (2018). Axon initial segments: structure, function, and disease. Ann. N Y Acad. Sci. *1420*, 46–61.

Ichida, J.K., and Kiskinis, E. (2015). Probing disorders of the nervous system using reprogramming approaches. EMBO J. *34*, 1456–1477.

Kaech, S., and Banker, G. (2006). Culturing hippocampal neurons. Nat. Protoc. *1*, 2406–2415.

Linda, K., Fiuza, C., and Nadif Kasri, N. (2018). The promise of induced pluripotent stem cells for neurodevelopmental disorders. Prog. Neuropsychopharmacol. Biol. Psychiatry *84* (*Pt B*), 382–391.

Lipstein, N., Verhoeven-Duif, N.M., Michelassi, F.E., Calloway, N., van Hasselt, P.M., Pienkowska, K., van Haaften, G., van Haelst, M.M., van Empelen, R., Cuppen, I., et al. (2017). Synaptic UNC13A protein variant causes increased neurotransmission and dyskinetic movement disorder. J. Clin. Invest. *127*, 1005–1018.

Mandolesi, G., Gentile, A., Musella, A., Fresegna, D., De Vito, F., Bullitta, S., Sepman, H., Marfia, G.A., and Centonze, D. (2015). Synaptopathy connects inflammation and neurodegeneration in multiple sclerosis. Nat. Rev. Neurol. *11*, 711–724.

Meijer, M., Burkhardt, P., de Wit, H., Toonen, R.F., Fasshauer, D., and Verhage, M. (2012). Munc18-1 mutations that strongly impair SNARE-complex binding support normal synaptic transmission. EMBO J. *31*, 2156–2168.

Meijer, M., Cijsouw, T., Toonen, R.F., and Verhage, M. (2015). Synaptic effects of Munc18-1 alternative splicing in excitatory hippocampal neurons. PLoS ONE *10*, e0138950.

Meijer, M., Dörr, B., Lammertse, H.C., Blithikioti, C., van Weering, J.R., Toonen, R.F., Söllner, T.H., and Verhage, M. (2018). Tyrosine phosphorylation of Munc18-1 inhibits synaptic transmission by preventing SNARE assembly. EMBO J. *37*, 300–320.

Mennerick, S., Que, J., Benz, A., and Zorumski, C.F. (1995). Passive and synaptic properties of hippocampal neurons grown in microcultures and in mass cultures. J. Neurophysiol. *73*, 320–332.

Mertens, J., Wang, Q.W., Kim, Y., Yu, D.X., Pham, S., Yang, B., Zheng, Y., Diffenderfer, K.E., Zhang, J., Soltani, S., et al.; Pharmacogenomics of Bipolar Disorder Study (2015). Differential responses to lithium in hyperexcitable neurons from patients with bipolar disorder. Nature *527*, 95–99.

Miller, G. (2010). Is pharma running out of brainy ideas? Science *329*, 502–504.

Na, J., Baker, D., Zhang, J., Andrews, P.W., and Barbaric, I. (2014). Aneuploidy in pluripotent stem cells and implications for cancerous transformation. Protein Cell *5*, 569–579.

Nehme, R., Zuccaro, E., Ghosh, S.D., Li, C., Sherwood, J.L., Pietilainen, O., Barrett, L.E., Limone, F., Worringer, K.A., Kommineni, S., et al. (2018). Combining NGN2 programming with developmental patterning generates human excitatory neurons with NMDAR-mediated synaptic transmission. Cell Rep. *23*, 2509–2523.

Pawlowski, M., Ortmann, D., Bertero, A., Tavares, J.M., Pedersen, R.A., Vallier, L., and Kotter, M.R.N. (2017). Inducible and deterministic forward programming of human pluripotent stem cells into neurons, skeletal myocytes, and oligodendrocytes. Stem Cell Reports *8*, 803–812.

Pfrieger, F.W. (2009). Roles of glial cells in synapse development. Cell. Mol. Life Sci. *66*, 2037–2047.

Qi, Y., Zhang, X.J., Renier, N., Wu, Z., Atkin, T., Sun, Z., Ozair, M.Z., Tchieu, J., Zimmer, B., Fattahi, F., et al. (2017). Combined small-molecule inhibition accelerates the derivation of functional cortical neurons from human pluripotent stem cells. Nat. Biotechnol. *35*, 154–163.

Qian, K., Huang, C.T., Chen, H., Blackbourn, L.W., 4th, Chen, Y., Cao, J., Yao, L., Sauvey, C., Du, Z., and Zhang, S.C. (2014). A simple and efficient system for regulating gene expression in human pluripotent stem cells and derivatives. Stem Cells *32*, 1230–1238.

Rhee, H.J., Shaib, A.H., Rehbach, K., Lee, C., Seif, P., Thomas, C., Gideons, E., Guenther, A., Krutenko, T., Hebisch, M., et al. (2019). An Autaptic Culture System for Standardized Analyses of iPSC-Derived Human Neurons. Cell Rep. *27*, this issue, 2212–2228.

Sanders, S.J., He, X., Willsey, A.J., Ercan-Sencicek, A.G., Samocha, K.E., Cicek, A.E., Murtha, M.T., Bal, V.H., Bishop, S.L., Dong, S., et al.; Autism Sequencing Consortium (2015). Insights into autism spectrum disorder genomic architecture and biology from 71 risk loci. Neuron *87*, 1215–1233.

Schmitz, S.K., Hjorth, J.J., Joemai, R.M., Wijntjes, R., Eijgenraam, S., de Bruijn, P., Georgiou, C., de Jong, A.P., van Ooyen, A., Verhage, M., et al. (2011). Automated analysis of neuronal morphology, synapse number and synaptic recruitment. J. Neurosci. Methods *195*, 185–193.

Schmitz, S.K., King, C., Kortleven, C., Huson, V., Kroon, T., Kevenaar, J.T., Schut, D., Saarloos, I., Hoetjes, J.P., de Wit, H., et al. (2016). Presynaptic inhibition upon CB1 or mGlu2/3 receptor activation requires ERK/MAPK phosphorylation of Munc18-1. EMBO J. *35*, 1236–1250.

Schubert, J., Siekierska, A., Langlois, M., May, P., Huneau, C., Becker, F., Muhle, H., Suls, A., Lemke, J.R., de Kovel, C.G., et al.; EuroEPINOMICS RES Consortium (2014). Mutations in STX1B, encoding a presynaptic protein, cause fever-associated epilepsy syndromes. Nat. Genet. *46*, 1327–1332.

Shcheglovitov, A., Shcheglovitova, O., Yazawa, M., Portmann, T., Shu, R., Sebastiano, V., Krawisz, A., Froehlich, W., Bernstein, J.A., Hallmayer, J.F., and Dolmetsch, R.E. (2013). SHANK3 and IGF1 restore synaptic deficits in neurons from 22q13 deletion syndrome patients. Nature *503*, 267–271.

Shen, X.M., Selcen, D., Brengman, J., and Engel, A.G. (2014). Mutant SNAP25B causes myasthenia, cortical hyperexcitability, ataxia, and intellectual disability. Neurology *83*, 2247–2255.

Shi, Y., Kirwan, P., and Livesey, F.J. (2012a). Directed differentiation of human pluripotent stem cells to cerebral cortex neurons and neural networks. Nat. Protoc. *7*, 1836–1846.

Shi, Y., Kirwan, P., Smith, J., Robinson, H.P., and Livesey, F.J. (2012b). Human cerebral cortex development from pluripotent stem cells to functional excitatory synapses. Nat. Neurosci. *15* (*3*), 477–486, S1.

Stamberger, H., Nikanorova, M., Willemsen, M.H., Accorsi, P., Angriman, M., Baier, H., Benkel-Herrenbrueck, I., Benoit, V., Budetta, M., Caliebe, A., et al. (2016). STXBP1 encephalopathy: a neurodevelopmental disorder including epilepsy. Neurology *86*, 954–962.

Südhof, T.C. (2013). Neurotransmitter release: the last millisecond in the life of a synaptic vesicle. Neuron *80*, 675–690.

Tarpey, P.S., Smith, R., Pleasance, E., Whibley, A., Edkins, S., Hardy, C., O'Meara, S., Latimer, C., Dicks, E., Menzies, A., et al. (2009). A systematic, large-scale resequencing screen of X-chromosome coding exons in mental retardation. Nat. Genet. *41*, 535–543.

Testa-Silva, G., Verhoog, M.B., Goriounova, N.A., Loebel, A., Hjorth, J., Baayen, J.C., de Kock, C.P., and Mansvelder, H.D. (2010). Human synapses show a wide temporal window for spike-timing-dependent plasticity. Front. Synaptic Neurosci. *2*, 12.

Testa-Silva, G., Verhoog, M.B., Linaro, D., de Kock, C.P., Baayen, J.C., Meredith, R.M., De Zeeuw, C.I., Giugliano, M., and Mansvelder, H.D. (2014). High bandwidth synaptic communication and frequency tracking in human neocortex. PLoS Biol. *12*, e1002007.

Toonen, R.F., Wierda, K., Sons, M.S., de Wit, H., Cornelisse, L.N., Brussaard, A., Plomp, J.J., and Verhage, M. (2006). Munc18-1 expression levels control

synapse recovery by regulating readily releasable pool size. Proc. Natl. Acad. Sci. U S A *103*, 18332–18337.

Varoqueaux, F., Jamain, S., and Brose, N. (2004). Neuroligin 2 is exclusively localized to inhibitory synapses. Eur. J. Cell Biol. *83*, 449–456.

Verhage, M., Maia, A.S., Plomp, J.J., Brussaard, A.B., Heeroma, J.H., Vermeer, H., Toonen, R.F., Hammer, R.E., van den Berg, T.K., Missler, M., et al. (2000). Synaptic assembly of the brain in the absence of neurotransmitter secretion. Science *287*, 864–869.

von Spiczak, S., Helbig, K.L., Shinde, D.N., Huether, R., Pendziwiat, M., Lourenço, C., Nunes, M.E., Sarco, D.P., Kaplan, R.A., Dlugos, D.J., et al.; Epi4K Consortium; EuroEPINOMICS-RES NLES Working Group (2017). *DNM1* encephalopathy: a new disease of vesicle fission. Neurology *89*, 385–394.

Wang, H., Hu, L., Liu, C., Su, Z., Wang, L., Pan, G., Guo, Y., and He, J. (2016). 5-HT2 receptors mediate functional modulation of GABAa receptors and inhibitory synaptic transmissions in human iPS-derived neurons. Sci. Rep. *6*, 20033.

Wang, C., Ward, M.E., Chen, R., Liu, K., Tracy, T.E., Chen, X., Xie, M., Sohn, P.D., Ludwig, C., Meyer-Franke, A., et al. (2017). Scalable production of iPSC-derived human neurons to identify tau-lowering compounds by high-content screening. Stem Cell Reports *9*, 1221–1233.

Wen, Z., Nguyen, H.N., Guo, Z., Lalli, M.A., Wang, X., Su, Y., Kim, N.S., Yoon, K.J., Shin, J., Zhang, C., et al. (2014). Synaptic dysregulation in a human iPS cell model of mental disorders. Nature *515*, 414–418.

Wierda, K.D., Toonen, R.F., de Wit, H., Brussaard, A.B., and Verhage, M. (2007). Interdependence of PKC-dependent and PKC-independent pathways for presynaptic plasticity. Neuron *54*, 275–290.

Zhang, Y., Pak, C., Han, Y., Ahlenius, H., Zhang, Z., Chanda, S., Marro, S., Patzke, C., Acuna, C., Covy, J., et al. (2013). Rapid single-step induction of functional neurons from human pluripotent stem cells. Neuron *78*, 785–798.

Zoghbi, H.Y., and Bear, M.F. (2012). Synaptic dysfunction in neurodevelopmental disorders associated with autism and intellectual disabilities. Cold Spring Harb. Perspect. Biol. *4*, a009886.

STAR★METHODS

KEY RESOURCES TABLE

REAGENT or RESOURCE	SOURCE	IDENTIFIER
Antibodies		
Mouse monoclonal anti-GFAP	Sigma	Cat#G3893; RRID:AB_477010
Chicken polyclonal anti-MAP2	Abcam	Cat#Ab5392; RRID:AB_2138153
Guinea pig polyclonal anti-Homer1	SYSY	Cat#160 004; RRID:AB_10549720
Rabbit polyclonal pan-Synapsin	Hosaka and Südhof, 1999	Cat#E028; RRID:AB_2315400
Mouse monoclonal anti-Ankyrin-G	NeuroMab	Cat#75-146; RRID:AB_10673030
Guinea Pig polyclonal anti-Synaptophysin	SYSY	Cat#101 004; RRID:AB_1210382
Mouse monoclonal anti-Pan-Axonal Neurofilament marker (SMI-312R)	Covance	Cat#SMI-312R; RRID:AB_2314906
Guinea Pig anti-VGAT	SYSY	Cat#131 004; RRID:AB_887873
Rabbit anti-Neuroligin2	Custom ordered at GenScript	Cat#SC1031
Mouse monoclonal anti-BRN2	Santa Cruz	Cat#sc-393324; RRID:AB_2737347
Rabbit polyclonal anti-BRN2	Abcam	Cat#ab94977; RRID:AB_10859580
Rat monoclonal anti-CTIP2	Abcam	Cat#ab18465; RRID:AB_2064130
Rabbit polyclonal anti- FOXG1	Abcam	Cat# ab18259; RRID:AB_732415
Mouse monoclonal anti-GABA	Sigma	Cat#A0310; RRID:AB_476667
Rabbit polyclonal anti-GABA	Sigma	Cat#A2052; RRID:AB_477652
Mouse monoclonal anti-SATB2	Abcam	Cat# ab92446; RRID:AB_10563678
Mouse monoclonal anti-TUJ1/β3-tubulin	Covance	Cat# MMS-435P; RRID:AB_2313773
Rabbit polyclonal anti-TUJ1/β3-tubulin	Covance	Cat# PRB-435P; RRID:AB_291637
Chicken polyclonal anti-TUJ1/β3-tubulin	Millipore	Cat# AB9354; RRID:AB_570918
Rabbit polyclonal anti-vGlut2	Abcam	Cat# ab84103; RRID:AB_10674784
Mouse monoclonal TRA1-81	Millipore	Cat# MAB4381; RRID:AB_177638
Bacterial and Virus Strains		
One Shot TOP10 chemically competent e. coli	Thermo Fisher	Cat#C404010
Chemicals, Peptides, and Recombinant Proteins		
Accutase	GIBCO	Cat#A11105-01
agarose type II-A	Sigma	Cat#A9918; CAS: 9012-36-6
DAPT	Sigma	Cat#D5942
Doxycycline	Sigma	Cat#D9891
EDTA	Sigma	Cat#E6635
Recombinant Human FGF	R&D systems	233-FB
Laminin	Sigma	Cat#L2020
LDN-193189	Axon Medchem	Cat# 1509
Poly-D-lysine	Sigma	Cat#P6407
Rat tail collagen	BD Biosciences	Cat# 354236
AraC	Sigma	Cat#C1768
BDNF	Stemcell technologies Peprotech	Cat#78005.3 Cat#450-10
NT3	Stemcell technologies	Cat#78074.1
Rho kinase (ROCK) inhibitor Y-27632	Abcam Tocris	Cat#ab120129; CAS 129830-38-2 Cat#1254
Picrotoxin	Abcam	Cat#ab120315
DNQX	Tocris	Cat#0189
D-AP5; D-(-)-2-Amino-5-phosphonopentanoic acid	R&D systems	Cat#0106
SB431542	Axon Medchem	Cat# 1661
Trehalose	Sigma	Cat#T9531

(*Continued on next page*)

Continued

REAGENT or RESOURCE	SOURCE	IDENTIFIER
Critical Commercial Assays		
TaqMan hPSC Scorecard Kit	Thermo Fisher Scientific	Cat#A15872
Human iPSC lines:		
C-35 m –r1 NGN2 iPSCs (generation of NGN2 neurons: 3 batches)	Generated in this study	N/A
C-14 m-s11 NGN2 iPSCs (generation of NGN2 neurons: 5 batches)	Generated in this study	N/A
C-62 m-s4 iPSCs (generation of GABA neurons: 3 batches)	Rehbach et al., in revision	N/A
C-61f-s2 iPSCs (generation of GABA neurons: 3 batches)	Rehbach et al., in revision	N/A
Experimental Models: Organisms/Strains		
Rat: Wistar (Crl:WI)	Charles River	Strain code: 003
Mouse*: munc18-1* null	Verhage et al., 2000	N/A
Oligonucleotides		
AAVS1 Forward: ACCAACGCCGACGGTATCAG	N/A	N/A
AAVS1 Reverse1: CAGACCCTTGCCCTGGTGGT	N/A	N/A
AAVS1 Reverse2: CACCAGGATCAGTGAAACGC	N/A	N/A
Recombinant DNA		
AAVS1-GFP	Dr. Su-Chun Zhang (University of Wisconsin) (Qian et al., 2014)	https://doi.org/10.1002/stem.1653
AAVS1-NGN2	Generated in this study	N/A
AAVS1-TALEN-L	Dr. Su-Chun Zhang (University of Wisconsin) (Qian et al., 2014)	https://doi.org/10.1002/stem.1653
AAVS1-TALEN-R	Dr. Su-Chun Zhang (University of Wisconsin) (Qian et al., 2014)	https://doi.org/10.1002/stem.1653
Software and Algorithms		
iPsychCNV package	Bertalan, 2017	https://biopsyk.dk/ipsychcnv/
plink 2.0	Chang et al., 2015	www.cog-genomics.org/plink/2.0/
MATLAB R2018a	MathWorks	https://mathworks.com
SynD – Synapse and neurite detection	Schmitz et al., 2011	https://www.johanneshjorth.se/SynD/SynD.html
INCell Analyzer 2200 software	GE Healthcare	https://www.gelifesciences.com/en/de/shop/cell-imaging-and-analysis/high-content-analysis-systems/instruments/in-cell-analyzer-2200-p-00558
INCell developer toolbox	GE Healthcare	https://www.gelifesciences.com/en/de/shop/cell-imaging-and-analysis/high-content-analysis-systems/instruments/in-cell-analyzer-2200-p-00558
GenomeStudio	Illumina	https://www.illumina.com/techniques/microarrays/array-data-analysis-experimental-design/genomestudio.html

CONTACT FOR REAGENT AND RESOURCE SHARING

Further information and requests for resources and reagents should be directed to and will be fulfilled by the Lead Contact, Matthijs Verhage (matthijs@cncr.vu.nl). Questions relating to cell generation can be directly addressed to Michael Peitz, Core Facility Cell Programming, University of Bonn Medical Faculty, Bonn, Germany (peitz@uni-bonn.de).

EXPERIMENTAL MODEL AND SUBJECT DETAILS

Laboratory Animals

Newborn P0-P1 pups from pregnant female Wistar rats (Crl:WI, strain code 003) were used for glia preparations. Mouse neurons were obtained from *munc18-1* null mice (Verhage et al., 2000), which are stillborn and can be easily distinguished from wild-type or heterozygous littermates. E18 embryos were obtained by caesarean section of pregnant females from timed matings of heterozygous mice. Animals were housed and bred according to institutional, Dutch and U.S. governmental guidelines.

iPSC lines

All iPSC lines used in this study are listed in the Key Resource table. The use of these lines was approved by the Ethics Committee of the Medical Faculty of the University of Bonn (approval number 275/08), and informed written consent was obtained from the donors. All experiments were performed in accordance with German guidelines and regulations.

METHOD DETAILS

Plasmid cloning

The AAVS1-GFP plasmid and the corresponding TALEN pair were kindly provided by Dr. Su-Chun Zhang (University of Wisconsin) as described previously (Qian et al., 2014). To establish the AAVS1-NGN2 targeting construct, the GFP coding sequence was removed from the AAVS1-GFP plasmid and replaced with the human NGN2 coding sequence (NGN2 template was received from Dr. Chao Sheng) via HiFi assembly (New England Biolabs).

AAVS1 targeting

AAVS1-targeted iPSC-lines were generated by nucleofecting 3-4 million cells with the corresponding targeting plasmid (4 μg) together with the TALEN pair (0.5 μg each) using the Amaxa nucleofection kit V (Lonza) in combination with program B-023 after a preincubation step with 10 μM of the Rho-associated kinase inhibitor (Y-27632, Tocris) for 1 h. Nucleofected iPSCs were seeded on Geltrex-coated dishes (ThermoFisher Scientific) at low density in StemMACS iPS Brew (Miltenyi Biotec) with 10 μM ROCK inhibitor (RI) as well as 5 μM L755507. After 24 h, medium was replaced with StemMACS iPS Brew including 10 μM RI, and then renewed every other day. RI was supplemented until the formation of small puromycin-resistant colonies and excluded afterward. Puromycin selection (0.3 μg/ml) was started after 48h post-nucleofection and maintained for at least 7 days. Resistant colonies were picked, expanded and analyzed via genotyping PCR. Site-specific transgene insertion was validated by PCR using the following primer combination: fwd: 5′-ACCAACGCCGACGGTATCAG-3′, rv1: 5′-CAGACCCTTGCCCTGGTGGT-3′, rv2: 5′-CACCAGGATCAGT GAAACGC-3′.

Forward programming into glutamatergic neurons

Before the start of differentiation, iPSCs were maintained in StemMACS iPS-Brew (Miltenyi Biotec) and splitted with EDTA. To start differentiation, iPSCs were dissociated with accutase and seeded on geltrex-coated six-well plates at a density of 7.500 cells/cm^2 in StemMACS iPS-Brew. One day after seeding, the medium was switched to N2 medium (DMEM/F12, 1% N2 supplement) supplemented with 2 μg/ml doxycycline to induce NGN2 expression. On day 2, the cells were dissociated with accutase and plated on PO/laminin-coated T175 flasks at a density of 50.000 cells/cm^2. At this point, the medium was switched to NB/B27 medium (neurobasal medium, 2% B27 supplement, 1ml GlutaMax, 1-2 μg/ml laminin, 10ng/ml BDNF) supplemented with doxycycline. On day 3, 10 μM DAPT was added to the medium. DAPT remained in the medium from day 3 until day 10. To remove remaining proliferative cells, 5 μM AraC was added on day 6 and day 8. While largely following the protocol initially described by the Südhof group (Zhang et al., 2013), we found the following steps particularly useful for producing large cell batches for subsequent cryopreservation: First, we maintained dox induction of NGN2 until the day of cryopreservation. This closely follows the original protocol of the Südhof group (Zhang et al., 2013), where they used long-term dox induction until the end of the experiment whereas Wang et al. induced expression of mouse Ngn2 for 3 days only (Wang et al., 2017). Second, we blocked notch signaling with DAPT to accelerate and synchronize neuronal induction since the NGN2-mediated conversion is less efficient under high cell densities which are required to enable bulk production. DAPT has been used also by others to accelerate the formation of excitatory forebrain neurons (Qi et al., 2017). These subtle modification yield a large proportion of BRN2-positive neurons, similar to findings of Zhang et al. (Zhang et al., 2013), but different to Wang et al., where BRN2 RNA expression appears to be low (Wang et al., 2017). Third, we added AraC to eliminate any remaining dividing cells. This is in agreement with Zhang et al., who use AraC from day 2 onward until the end of the experiment, and also with Wang et al., who used AraC in selected experimental settings (Wang et al., 2017; Zhang et al., 2013).

On day 11, neurons were combined as a single batch and cryopreserved. Neuronal cultures were dissociated slowly by incubating accutase supplemented with 10μM RI for 60-90 minutes at 37°C. Cells were washed off with pre-warmed medium, dissociated further by pipetting and passed through a 40 μm cell strainer. The cell suspension was mixed, divided into several falcon tubes and centrifuged at 300 g for 5 min. Subsequently, the cells were resuspended in ice-cold freezing medium (70% KOSR, 20% 1M trehalose, 10% DMSO), aliquoted in vials of 0.2-1 mio cells and frozen with a rate of approximately −1°C per min. Cells remaining in the cell strainer were collected for DNA analysis.

Differentiation into GABAergic forebrain neurons

To generate an alternative, GABAergic forebrain differentiation, briefly, we seeded IPSCs that were maintained in E8 medium at a density of $0.2x10^6$ per cm^2 and switched medium to neural induction medium (N2/B27, 500nM LDN-193189, 15μM SB431542) the next day until day 10. On day 10, the cultures were split. 20ng/ml FGF2 were added from day 9 to day 12. On day 20, precursors were frozen and on day 27, neurons were frozen as large batch (for details, see article by Rhee et al., 2019 in the same issue of this journal).

Quality control

For QC, neurons were thawed, counted and seeded on 96-well plates (ibidi, μ-plates) in NB/B27 medium supplemented with 10 μM RI. After 7 days, neurons were fixed with freshly thawed pre-warmed 4% PFA for 10-15 minutes. For the fixation of GABA, the PFA solution was supplemented with 0.04% glutaraldehyde. Cultures were blocked with 10% FBS in PBS + 0.1% Triton X-100 for one hour. The primary antibodies were diluted in 10% FBS in PBS + 0.1% Triton X-100 and incubated over night at 4°C. Afterward, adequate secondary antibodies were diluted in 10% FBS in PBS + 0.1% Triton X-100 and incubated for one hour. The following antibodies were used: BRN2 (ms IgG, Santa Cruz, sc-393324, 1:500; rb IgG, abcam 94977, 1:500), CTIP2 (rat IgG, abcam, ab18465, 1:500), GABA (ms IgG, Sigma, A0310, 1:1000; rb IgG, Sigma, A2052, 1:1000), SATB2 (ms IgG, abcam, ab92446, 1:100), TUJ1 (β3-tubulin, ms IgG, Covance, MMS-435P, 1:1000; rb IgG, Covance, PRB-435P, 1:2000; ck IgY, Millipore, AB9354, 1:500), vGlut2 (rb IgG, abcam ab84103, 1:500), FOXG1 (rb IgG, abcam, ab18259, 1:500). Images were acquired using the IN Cell Analyzer 2000 (GE Healthcare). Cellular markers were quantified automatically using the InCell Developer toolbox.

SNP analysis and CNV calling

For SNP analysis, DNA was prepared using the QIAGEN DNeasy Blood & Tissue kit. Samples were processed by the LIFE&BRAIN GmbH Genomics platform at the Institute of Human Genetics at the University of Bonn on the Illumina Infinium PsychArray or the Infinium Global Screening Array (GSA). The generated SNP data was processed and annotated with the Illumina Genome Studio software. CNV calling was performed using the iPsychCNV package in R, which incorporates information about the B allele frequency distribution in addition to the Log R ratio to reduce the detection of false positives (for more details, see https://biopsyk.dk/ipsychcnv/ and Bertalan, 2017). All genes within CNVs greater than 500Kb (containing > 100 SNPs) were filtered against gene lists derived using brain development and synapse gene ontology (GO) terms. Samples showing overlap between genes affected by CNVs and genes on the GO term list were excluded. To prevent removal of samples with falsely discovered CNVs, Log R ratios and B allele frequencies were plotted and visually examined. In ambiguous cases, the CNVs were validated using genomic qPCR. The genetic relatedness between samples was obtained using plink 2.0 (Chang et al., 2015) (www.cog-genomics.org/plink/2.0/) and compared against all processed samples to validate genomic identity, which was set to be confirmed when having an overlap of > 90% of SNPs.

Microdot arrays

To achieve rat glia microdot arrays, glass coverslips (Menzel) were etched in 1M HCl for at least two hours and neutralized with 1M NaOH for maximum one hour, washed thoroughly with MilliQ water and once with 70% ethanol. Coverslips were stored in 96% ethanol and coated with agarose type II-A (0.0015% in H_20, Sigma) prior to microdot application. Coating was done by applying heated agarose (55°C) and removing it after 30 s leaving a thin layer of agarose solution over the entire coverslip. Microdots were created using a custom-made rubber stamp (dot diameter 250μm) to apply solution consisting of 0.1mg/ml poly-D-lysine (Sigma), 0.7mg/ml rat tail collagen (BD Biosciences) and 10mM acetic acid (Sigma) by stamping from a wet filter paper (3mm cellulose chromatography paper (Whatman)). Coverslips were UV-sterilized for 20 minutes before further use. Rat astrocytes were plated at 4-5K/well in pre-warmed DMEM medium (Lonza, LO BE12-604F/U1/12) supplemented with 10% heat-inactivated fetal calf serum (Life technologies, 10270), 1% nonessential amino acids (life technologies: 11140-035) and 1% penicillin/streptomycin (Life technologies, 15140-122). When glia islands reach confluence (after 5-6 days), medium is switched to neuronal medium. This approach yields microdots containing on average ~25-30 glia cells, irrespective of the amount of glia plated (Figure S6). For human neuron cultures, glia islands undergo AraC treatment (2μM, Sigma; C1768) for at least 24 hours prior to switching medium to neuronal medium containing Neurobasal (Life technologies, 21103-049) supplemented with 2% B27 (Life technologies, 17504-044), 1.8% HEPES (1M stock; Life technologies, 15630-056), 0.25% glutamax (100x stock, Life technologies, 35050-038) and 0.1% PenStrep (100x stock, Life technologies, 15140-122). For NGN2 neurons, the following growth factors were freshly added to the medium: 10ng/ml BDNF (Stemcell technologies, 78005.3) and 10ng/ml NT3 (Stemcell technologies, 78074.1). For classically differentiated GABAergic neurons, a different neuronal medium was used containing 50% DMEM/F12, 50% Neurobasal, 1% N2, 1% B27, 50μM B-mercaptoethanol, 1mM Glutamine and 0.5% NEAA. 1% HI-FCS (Life technologies, 10270) was added to the culture medium to ensure long-term survival of supporting glia cells.

Primary Mouse Neuron Culture

Hippocampi from *munc18-1* null mice were collected in ice-cold Hanks Buffered Salt Solution (HBSS; Sigma) buffered with 7mM HEPES (Life technologies). After removal of the meninges, neurons were incubated in Hanks-HEPES containing 0.25% trypsin (from 10x stock, Invitrogen) for 20 minutes at 37°C. After washing, neurons were triturated using a fire-polished Pasteur pipette

and counted in a Fuchs-Rosenthal chamber. To achieve autaptic cultures, hippocampal *munc18-1* null neurons were plated on micro-islands of rat glia at a density of 6K per well in a 12-well plate and infected with lentiviral particles encoding Munc18-1 several hours after plating.

Thawing and culture of cryopreserved human neurons

Cryopreserved human neurons are quickly thawed in a 37°C water bath and transferred to a 15ml tube. 10ml pre-warmed neuronal medium (without growth factors but supplemented with 5μM ROCK inhibitor (Abcam, ab120129)) was slowly added while shaking. Cells were resuspended using a 10ml pipette and passed through a 40μm cell strainer into 50ml tube. A small sample (20μl) was mixed with Trypan Blue to count viable cells and the remaining cells were plated at appropriate density (2K per well in a 12-well plate for induced Glutamatergic forebrain (NGN2) neurons and 0.75K for classic GABAergic forebrain neurons). Next day, 100% of medium (pH equilibrated) was refreshed. Next, 50% of neuronal medium was refreshed every 3-4 days.

Morphological analysis

Neurons were fixed with 3.7% formaldehyde (Electron Microscopy Sciences) in PBS for 20 minutes at room temperature (RT). Classic GABA neurons were fixed every 14 days starting at DIV30 (week 4+2), and NGN2 neurons at DIV14, 27, 31, 35 and 45. Cells were permeated with 0.5% Triton X-100 for 5 min and blocked with 2% normal goat serum (NGS, Life Technologies) and 0.1% Triton X-100 for 30-60 minutes. For AnkyrinG stainings, 10% NGS was used for blocking. Cells were incubated for 1-2 h at RT in 2% NGS and 0.1% Triton X-100 mixed with primary antibodies. After washing with PBS, cells were incubated for 1 h at room temperature with secondary antibodies conjugated to Alexa dyes (1:1000, Invitrogen Molecular Probes), washed again and mounted with DABCO-Mowiol (Invitrogen). To assess the number of glia cell nuclei per microdot, TO-PRO-3 Iodide (1:5000, Molecular Probes, T-3606) was added to the secondary antibody mix to visualize nuclei.

The following primary antibodies were used: monoclonal mouse GFAP (1:1000, Sigma, G3893), polyclonal chicken anti-MAP2 (1:500 or 1:1000, Abcam, ab5392), polyclonal guinea pig anti-Homer1 (1:300, SYSY #160004), polyclonal rabbit SynapsinI/II (1:1000, kind gift from T. Südhof; Hosaka and Südhof, 1999), monoclonal mouse anti-Ankyrin-G (1:750 or 1:1000, NeuroMab, cat# 75-146), polyclonal guinea pig anti-Synaptophysin1 (1:500, SYSY #101004), monoclonal mouse antibody against Pan-Axonal Neurofilament marker (1:1000, Covance, cat# SMI-312R), polyclonal guinea pig anti-VGAT (1:500, SYSY #131004) and rabbit anti-Neuroligin2 (1:100, GenScript #700031-7).

Images were acquired with (Figures 2 and S2) a confocal microscope (Nikon Eclipse Ti) equipped with a 40 × oil (numerical aperture [NA] = 1.3) objective (no zoom) controlled by NisElements 4.30 software or (Figures 6 and S1) LSM 510 (Carl Zeiss) using a 40x oil immersion objective (NA = 1.3) with 0.7x zoom. Confocal settings were kept the same for all scans within a culture. For Figure S2, complete microdots were imaged using 3x3 imaging with a 40x oil objective and automated stitching. Maximum intensity projections of 3 z-planes were made using open source software ImageJ. Images were analyzed in MATLAB with SynD, an automated image analysis routine (Schmitz et al., 2011). In short, the software uses thresholding of the MAP2 image to detect soma. Starting from the soma, a neurite tracing algorithm is used to complete the morphology mask, from which dendrite length is calculated. Synaptic puncta are detected using thresholding of the synapse marker, requiring putative synapses to be above the mean synapse channel intensity by a (manually set) number of standard deviations. Pixels outside the neurite mask or on the soma are excluded. Also, regions smaller than a manually set area size are excluded. From the resulting synapse mask, synapse numbers and intensity are calculated. For Figure 2, synapse detection settings were optimized for each time point per culture. For Figure S2, synapse detection settings were optimized for the latest time-point per culture.

Synapse physiology

Whole-cell voltage-clamp recordings (Vm = −70mV) were performed at room temperature with borosilicate glass pipettes (2.5-4.5 MOhm) filled with 125mM K-Gluconate, 10mM NaCl, 4.6mM $MgCl_2$, 4mM K2-ATP, 15mM creatine phosphate, 10U/ml phosphocreatine kinase and 1mM EGTA (pH 7.30, 290 mOsmol). External solution contained the following (in mM): 10 HEPES, 10 Glucose, 140 NaCl, 2.4 KCl, 4 $MgCl_2$ and 4 $CaCl_2$ (pH = 7.30, 300 mOsmol). Excitatory and inhibitory neurons were distinguished on basis of their postsynaptic decay kinetics. Recordings were performed with Axopatch 200A/200B amplifiers (Molecular Devices), Digidata 1322A/1440 and Clampex 9.0/10.0 software (Molecular Devices). Action potentials were elicited by a 1ms depolarization to 30 mV. Only cells with successful action potential generation and leak current of < 500 pA were accepted for analysis. NMDA currents were recorded in Mg-free aCSF (158mM NaCl, 2.4mM KCl, 4mM $CaCl^2$, 10mM HEPES, 10mM glucose, 100 μm picrotoxin, 100 μm glycine (pH 7.3, 315mOsm)). Resting membrane potential was assessed in current-clamp immediately after break-in. Bath application of 40 μM DNQX was used to delineate NMDAR-mediated currents in EPSCs larger than 800pA. Subsequent addition of 100 uM AP-V blocked the entire glutamatergic responses. AMPAR-mediated currents were calculated by subtracting NMDAR-mediated currents from the Mg-free total current averaged over 2 pulses at 0.5Hz.

Offline analysis was performed using custom-written software routines in MATLAB R2018a (Mathworks). Stimulation artifacts were removed and interpolated using cubic interpolation.

QUANTIFICATION AND STATISTICAL ANALYSIS

Statistical analysis of electrophysiological data was performed with Instat v3.05 software (GraphPad). Data samples were first tested for normality with the Kolmogorov and Smirnov test and for heterogeneity of variance with the method of Bartlett. If data allowed an unpaired t test (with Welch correction if standard deviations were not equal) was used to determine statistical significance. If data failed to pass the normality test, the non-parametric Mann-Whitney U test was used. Morphological data in Figure S2 was analyzed as follows: data samples were first tested for normality with the Shapiro-Wilk normality test. If data failed to pass the normality test, the Kruskal-Wallis test with Dunn's multiple comparisons test was used. P values below 0.05 are considered significant and are indicated as following: *$p < 0.05$, ** $p < 0.01$, *** $p < 0.001$. Statistical details can be found in the figure legends.